Improved Turbulence Profiling with Field-Adapted Acoustic Doppler Velocimeters Using a Bifrequency Doppler Noise Suppression Method

D. HURTHER

Laboratoire des Ecoulements Géophysiques et Industriels, CNRS UMR 5519, Grenoble, France

U. LEMMIN

Laboratoire d'Hydraulique Environnementale, Ecole Polytechnique Fédérale de Lausanne, Lausanne, Switzerland

(Manuscript received 7 July 2006, in final form 8 February 2007)

ABSTRACT

A novel noise reduction method and corresponding technique are presented for improving turbulence measurements with acoustic Doppler velocimeters (ADVs) commonly used in field studies of coastal and nearshore regions, rivers, lakes, and estuaries. This bifrequency method is based on the decorrelation of the random and statistically independent Doppler noise terms contained in the Doppler signals at two frequencies. It is shown through experiments in an oscillating grid turbulence (OGT) tank producing diffusive isotropic turbulence that a shift in carrier frequency of less than 10% is sufficient to increase the resolved frequency range by a decade in the turbulent velocity spectra. Over this spectral range, the slope of the velocity spectra agrees well with the universal inertial range value of −5/3. The limit due to spatial averaging effects over the sample volume can be determined from the abrupt deviation of the spectral slope from the −5/3 value. As a result, the relative error of the turbulent intensity estimate and the turbulent kinetic energy (TKE) dissipation rate, measured by two different methods, does not exceed 10% in the case of isotropic turbulence. Furthermore, the bifrequency method allows accurate estimates of the turbulent microscales as shown by the good agreement of the ratio between the Taylor and Kolmogorov microscales and an $\mathrm{Re}_t^{1/4}$ power law. Compared to previous Doppler noise reduction methods (Garbini et al.), an increase in time resolution by a factor of 4 is achieved. The proposed method also avoids the loss of TKE energy contained in isotropic flow structures of size equal to and smaller than the sample volume. Different from Doppler noise methods proposed by Hurther and Lemmin and Blanckaert and Lemmin, this method does not require additional hardware components, electronic circuitry, or sensors because the redundant instantaneous velocity field information is captured with the same transducer. The required shift in carrier frequency is small enough for the bifrequency method to be easily implemented in commercial ADVs.

1. Introduction

Over the past two decades, field studies of small-scale processes involving turbulence have benefited from the development of high-resolution acoustic Doppler velocimeters (ADVs) and ADV profilers (ADVPs) working in pulse-to-pulse coherent mode (Hay and Sheng 1992; Lhermitte and Lemmin 1994; Zedel et al. 1996; Voulgaris and Trowbridge 1998; López and Garcia 1999; Hurther and Lemmin 2000, 2003; Nikora and Goring 2000; Trowbridge and Elgar 2001; Hoefel and Elgar 2003; Zappa et al. 2003; Blanckaert and De Vriend 2004; Davies and Thorne 2005; Elgar et al. 2005; Betteridge et al. 2006). Examples include hydrodynamic, biogeochemical, morphodynamic, and sediment transport studies in estuaries, rivers, lakes, and nearshore and coastal regions. They successfully explain small-scale coupling phenomena between the flow and a reacting phase, since they are able to investigate finescale dynamics well into the turbulent production range and a fraction of the inertial subrange.

ADVs are well designed for direct shear Reynolds stress measurements in bed-shear-dominated turbulence as is found in rivers or macrotidal estuaries (Lane et al. 1998; Kim et al. 2000; Nikora and Goring 2000; Zappa et al. 2003). They are less accurate in estimating the normal Reynolds stress components, the turbulent

Corresponding author address: D. Hurther, Laboratoire des Ecoulements Géophysiques et Industriels, CNRS UMR 5519, Grenoble, France.
E-mail: david.hurther@hmg.inpg.fr

DOI: 10.1175/2007JTECHO512.1

kinetic energy (TKE) dissipation range, and the turbulent microscales in diffusive isotropic turbulence as is observed in nearshore zones affected by wave breaking–induced turbulence (Hurther et al. 2007; Sénéchal et al. 2002; Elgar et al. 2005) because they can only resolve a limited fraction of the inertial subrange. This is due to the inherent contribution of random Doppler phase noise, which cannot be suppressed when calculating normal Reynolds quantities. As a result, the TKE, the TKE dissipation rate, and the turbulent microscales are also affected by important noise levels, which can lead to wrong data interpretations.

Two types of physical noise in acoustic backscattering system (ABS) signals can be distinguished. The first one results from the lack of acoustic targets in the sample volume as is found in the calm waters of dead zones or lakes. Furthermore, the temporary presence of air bubbles between the emitter and receiver can reflect most of the incident acoustic pressure contained in the pulse train. This can occur in breaking waves at the air/water interface or in hydraulic jumps. As a consequence, certain receivers may capture an acoustic echo, but others may not. This type of noise is characterized by the presence of intermittent peaks in the velocity time series. Since this noise occurs in poor measurement environments, it is not inherent to the measuring principle of ADVs. The method proposed here does not deal with this problem.

This study addresses the second type of noise, which is the Doppler noise effect inherent to the measuring principle (Garbini et al. 1982; Loupas and Gill 1994). It occurs in the presence of a sufficiently large number of acoustic targets homogeneously distributed in the sample volume (micro-air bubbles or suspended matter). The random target distribution in the sample volume induces an instantaneous Lagrangian deviation of the target's position from the mean position determined by the spatially averaged velocity. This creates an instantaneous random Doppler noise phase that is added to the spatially averaged Doppler phase. This random process is inherent to the measuring principle and occurs even under "excellent" working conditions.

The advantages of a new Doppler noise reduction method applied to velocity profile measurements in an isotropic turbulent flow field will be demonstrated. The experiments are conducted in an oscillating grid tank. Well-established semitheoretical expressions will be applied to calculate accurate reference values. The choice of oscillating grid turbulence (OGT) is deliberate in order to generate a shear-free turbulent flow field, because, as mentioned earlier, it is difficult to precisely investigate this type of turbulence using pulse-coherent ADVs.

2. Oscillating grid experiment

This investigation is conducted in an oscillating grid tank for two reasons. First, by using well-established semiempirical and/or analytical models of the literature as reference, it provides for a rigorous validation of the measurements with and without the proposed correction method. The following sections will briefly discuss the experimental setup, the associated flow regimes, and the literature results on OGT.

Second, pulsed ADVs have a limited ability to measure normal Reynolds stresses in a fully isotropic turbulent flow (Voulgaris and Trowbridge 1998; Hurther and Lemmin 2001). The high degree of isotropy and stationarity provided by OGT is therefore ideal for testing the efficiency of the proposed Doppler noise correction method.

a. Oscillating grid turbulence

Experiments in an oscillating grid tank allow generating a stationary, isotropic, and turbulent flow field outside the near field of the vertically oscillating grid. The far field is the region above the near field with a high degree of flow isotropy in which the grid signature can no longer be distinguished. Hopfinger and Toly (1976) estimated a degree of isotropy between the three components of turbulent intensities above 95%. The strong inhomogeneity of the turbulence quantities in the vertical direction is due to the high decay of transport by turbulent diffusion, which is balanced locally by the TKE dissipation rate. Since the flow regime is well controlled, no mechanism other than TKE dissipation is at the origin of that decay.

To quantify the effects of the proposed correction method on the estimate of the turbulent quantities, the present analysis requires reference values for these quantities. Several semitheoretical expressions for the TKE profiles and TKE dissipation rate exist in the literature (Hopfinger and Toly 1976; Ura et al. 1987; De Silva and Fernando 1992). Matsunaga et al. (1999) have derived analytical solutions from a $k - \varepsilon$ model that showed very good agreement with all of the previously proposed semitheoretical formulas. The parameterized form of the solutions for the TKE and TKE dissipation rate are

$$\frac{k}{k_0} = \left(\frac{1}{1.82}\frac{z}{z_0} + 1\right)^{-5}, \tag{1}$$

$$\frac{\varepsilon}{\varepsilon_0} = \left(\frac{1}{1.82}\frac{z}{z_0} + 1\right)^{-(17/2)}, \tag{2}$$

with k_0, ε_0, and $z_0 = k_0^{3/2}\varepsilon_0^{-1}$ being constants that depend on the grid Reynolds number [$\mathrm{Re} = (FS^2/\nu)$]; *F, S,*

and M are the oscillation frequency of the grid, the stroke, and the mesh size parameter. For Re $\leq$ 5500

$$\frac{k_0}{F^2S^2} = 8.1 \times 10^{-3}(S/M)^{1/4}\,\mathrm{Re}^{1/2},$$

$$\frac{\varepsilon_0}{F^3S^2} = 8.2 \times 10^{-5}(S/M)\,\mathrm{Re}, \qquad (3)$$

and for Re $\geq$ 5500

$$\frac{k_0}{F^2S^2} = 6 \times 10^{-1}(S/M)^{1/4},$$

$$\frac{\varepsilon_0}{F^3S^2} = 4.5 \times 10^{-1}(S/M). \qquad (4)$$

The analytical solution for k showed good agreement with all semiempirical expressions in a z/z_0 range restricted to the experimental conditions of Hopfinger and Toly (1976), Ura et al. (1987), and De Silva and Fernando (1992). Gratiot et al. (2005) have demonstrated the validity of the parameterized model solution by Matsunaga et al. (1999) over a much wider range in z/z_0 than the range covered in the earlier experiments. Therefore, Eqs. (3) or (4) will be used as reference for our measurements.

b. Experimental setup and flow regime

The tank and grid are designed to the specifications defined in Thompson and Turner (1975) and Hopfinger and Toly (1976), which are based on earlier tests with different grid geometries and tank dimensions (Rouse and Dodu 1955; Bouvard and Dumas 1967; Turner 1968). The tank is a square Plexiglas box, 53 cm wide and 90 cm high (Fig. 1). The grid is made of seven square bars in both horizontal directions. The thickness of the square bars is m = 1.5 cm with a mesh size of M = 7.5 cm. The ratio M/m = 5 corresponds to the standard ratio value, resulting in a grid porosity close to 65%. This geometrical configuration is found to minimize secondary circulation.

During the experiment, the water depth is H = 70 cm and the grid is fixed horizontally on a vertical steel bar guiding the vertical oscillation movement of the grid. The mean grid position is located 25 cm above the bottom of the tank. It oscillates at a controlled frequency of F = 4.65 Hz with a stroke (twice the amplitude) of S = 4 cm. The Reynolds number for the experiment is Re = 7400 and Eqs. (3) and (4) will be used for the calculation of the reference profiles for k and ε.

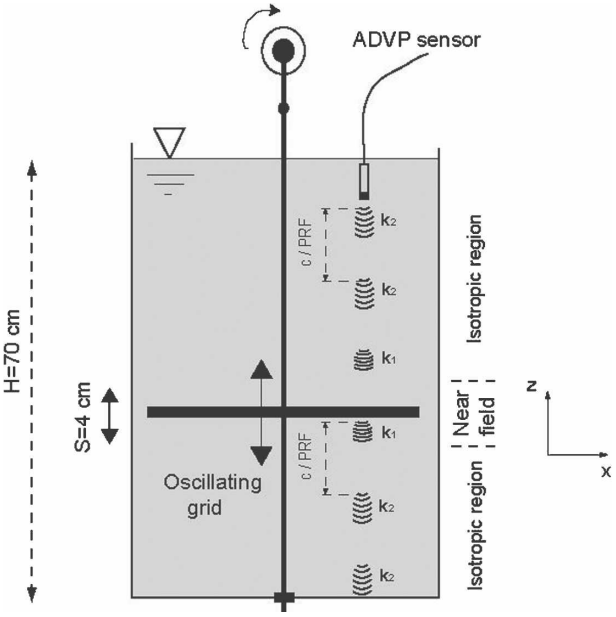

FIG. 1. The OGT tank. The transducer of the ADVP is placed below the free surface at half distance between the center and the sidewall.

3. A bifrequency ADV profiler

This ADVP can profile up to four different radial velocity components when it is configured in multistatic mode (Hurther and Lemmin 1998; Blanckaert and De Vriend 2004; Blanckaert and Lemmin 2006). However, the system here is configured as a monostatic device as sketched in Fig. 1, because the Doppler noise process is independent of the configuration. The bifrequency method can therefore also be applied to commercial ADVs with or without the profiling ability, in mono- or multistatic configuration. This is a major difference from previous Doppler noise reduction methods, which were based on a profiling ability (Garbini et al. 1982) or additional receivers (Hurther and Lemmin 2001; Blanckaert and Lemmin 2006). In existing commercial systems these Doppler noise reduction methods require important internal modifications in terms of hardware, hardware performance (much higher sampling rates), and software.

a. Modus operandi

A single emitter (piezzoelectrical transducer) is supplied with a signal composed of pairs of pulse trains with alternating carrier frequency, thus avoiding additional analog filters and associated channels in the hardware. The output signal with alternating carrier frequency can be demodulated in one single channel with exactly the same electrical characteristics as a stan-

dard single frequency signal. Furthermore, pairs of pulse trains are generated in order to maintain the same velocity range. The time lag between the pulses is constant and equal to 1.5 ms. This solution is appropriate as long as the time lag 4/PRF (pulse repetition frequency) is much shorter than the smallest turbulent time scale that needs to be resolved. In our case this time lag is equal to 6 ms, which is at least 5 times smaller than the highest resolved turbulence time scale.

This mode of operation allows the quasi-simultaneous reception of two echo pairs at two different carrier frequencies, k_1 and k_2, coming from the same sample volume. Two different bifrequency settings will be tested. The frequency shifts are $df_1 = 180$ and $df_2 = 240$ kHz for the frequency pairs 1.25/1.43 and 1.43/1.67 MHz, respectively. The shifts should not exceed the −6-dB bandwidth of the transducer in order to avoid any frequency coupling effects and to have a sufficiently high sensitivity and signal-to-noise ratio at all frequencies. Also, the relative difference in sample volume size at the two frequencies never exceeds 25% for the farthest gate in the profile. Technically, these conditions are fulfilled with standard piston transducers, since they correspond to a shift of 8% and 11% relative to the central frequency of the transducer.

b. Principles of ABS

In a monostatic configuration where the transducer is used as an emitter and a receiver, the backscattered pressure p_j at the transducer's face resulting from a single scatterer j located at a range r_j in the far field of the transducer is written as

$$p_j = A(r_j)\exp[i(\omega_c t + 2k_c r_j) + \zeta_j], \tag{5}$$

where ω_c, $k_c = 2\pi/\lambda_c$, and ζ are the carrier pulsation, the carrier wavenumber in water, and the random scattering phase. Here, $A(r_j)$ is the amplitude of the backscattered pressure:

$$A(r_i) = p_r r_r \frac{a_s}{2} f_s \frac{D^2}{r_j^2}\exp(-2\alpha r_j), \tag{6}$$

where p_r is the reference pressure at $r_r = 1$ m, a_s is the diameter of the scatterer, f_s is the form function representing the scattering properties of the acoustical target, D is the directivity function of the transducer, and α is the absorption coefficient in water. It is assumed that at any given time a large number N of scatterers is contained in the sample volume. Similar to Garbini et al. (1982), the position of each scatterer is decomposed as $r_j = r_{oj} + \hat{r} + \tilde{r}_j$, with r_{oj} being the initial position. Here, $\hat{r}(t) = \int_0^t \hat{u}(t)dt$ is the mean Lagrangian displacement associated with the mean scatterer velocity in the sample volume and $\tilde{r}_j(t) = \int_0^t [u_i(t) - \hat{u}(t)]dt$ is the Lagrangian drift from the mean displacement. In the following, $\langle\rangle$ denotes the sum over N scatterers contained in the sample volume. After applying a quadrature demodulation and a low-pass filtering to the received pressure signal, the measured pressure in the case of first-order scattering becomes

$$\langle p\rangle = \Omega\exp(i\gamma)\exp(ik_c\hat{r}),$$

$$\text{with}\quad \begin{cases} \Omega^2 = NA^2(r_j) + \displaystyle\sum_{\substack{j=1,k=1\\ j\neq k}}^{N} A(r_j)A(r_k)[\sin(\varphi_j)\sin(\varphi_k) + \cos(\varphi_j)\cos(\varphi_k)] \\ \gamma = \arctan\left[\dfrac{-\displaystyle\sum_{j=1}^{N} A(r_j)\sin(\varphi_j)}{\displaystyle\sum_{j=1}^{N} A(r_j)\cos(\varphi_j)}\right] \end{cases} \tag{7}$$

$$\text{and}\quad \varphi_j = k_c(r_{oj} + \tilde{r}_j) + \zeta_j. \tag{8}$$

The second term on the rhs of the upper Eq. (7) and the term γ both represent undesired coupling effects between the scatterers in the sample volume. They can affect the amplitude and the phase of the measured pressure. The presence of the term $\tilde{r}_j$ in Eq. (8) is due to the effect of turbulence, because the mean Lagrangian displacement $\hat{r}$ is smaller than the turbulent macroscale of the flow. This is valid for most ADVs, since the size of the sample volume is on the order of $O(10^{-3}$ m) compared to the turbulent macroscale, which varies typically over $O(10^{-2}$ m)–$O(1$ m). If $\tilde{r}_j$ is statistically independent for the scatterers in the sample volume, the Lagrangian drift has the same effect as the incoherent scattering process due to the random distribution of the scatterer's position and the random scattering phase.

The statistical independence of $\tilde{r}_j$ is principally conditioned by the level of turbulence in the flow. It has to be high enough so that the scale of the flow that corresponds to the size of the sample volume is in the inertial range of the turbulent spectra. In this case, Lagrangian drifts are independent for the scatterers in the sample volume because of their isotropic properties. As a result, the idealized incoherent scattering and Lagrangian drift processes imply that the second term on the rhs of the upper Eq. (7) and the time fluctuation of term γ are negligible. This leads to the following simplification for the amplitude:

$$\Omega^2 = NA^2 = \int^{vol} MA^2\, d\vartheta \quad \text{with} \quad M = N/d\vartheta. \tag{9}$$

Since the volumetric concentration of the scatterers is homogeneous in the sample volume, the discrete sum over the number of scatterers is replaced by an integral over the sample volume with M being equal to the volumetric concentration. The result of this integration is known as the acoustic backscattering system equation. Its inversion allows one to estimate the mass concentration C in the sample volume. A thorough review of this measuring principle is given by Thorne and Hanes (2002). The measured electrical mean square voltage becomes

$$\begin{aligned}\langle \overline{V^2} \rangle &= (RT)^2\Omega^2, \\ &= \left[\left(\frac{RTp_r r_r}{1.05 k a_t \psi r} \right)^2 \frac{3}{16}\, \tau c \exp(-4\alpha r) \right] \left(\frac{\langle f_s \rangle^2}{\langle a_s \rangle \rho_s} \right) C,\end{aligned} \tag{10}$$

where R and T are constants for the transducer's sensitivity and electrical circuitry.

By neglecting the undesired coupling effect terms, the time derivative of the phase of the integrated pressure signal becomes proportional to the velocity that is spatially averaged over the sample volume:

$$\langle V \rangle = \frac{ck_c}{2\pi f_c} \frac{d}{dt} \hat{r}(t). \tag{11}$$

Figure 2 shows several velocity spectra for two carrier frequencies, $f_c = f_1 = 1.25$ MHz and $f_c = f_2 = 1.67$ MHz measured with the ADVP during the oscillating grid experiment. For the flow regime specified in section 2b, the measurement point is located at $z/z_0 = 0.9$ from the center of the grid. The velocity spectra are calculated from the Fourier transform of the temporal autocorrelation function of the velocity signal:

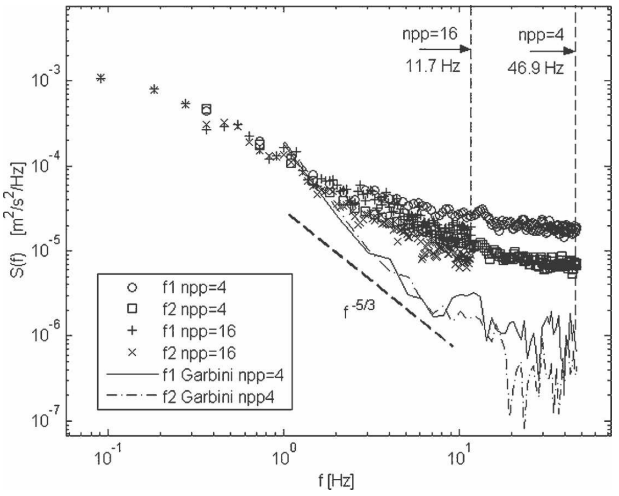

FIG. 2. Turbulent velocity spectra in the far field of the OGT tank. Points: standard method (i.e., without Doppler noise suppression for two carrier frequencies f_1 and f_2 and with two time resolutions). Lines: Doppler noise reduction method proposed by Garbini et al. (1982).

$$S_{VV}(f) = \int_{-\infty}^{+\infty} R_{VV}(\tau) \exp(-i2\pi f\tau)\, d\tau. \tag{12}$$

The parameter npp in Fig. 2 indicates the number of samples over which the consecutive velocity estimations are averaged using the pulse-pair algorithm (Hurther and Lemmin 2001).

As can be seen in Fig. 2, for $f > 3$ Hz, the slope of the spectra represented by the symbols deviates from the expected $-5/3$ slope (dashed line). The lower decay with frequencies above 3 Hz is due to the effect of the term γ on the velocity signal:

$$V = \frac{ck_c}{2\pi f_c} \frac{d}{dt} [\hat{r}(t) + \gamma(t)] = \langle V \rangle(t) + n(t). \tag{13}$$

The signal $n(t)$ is referred to as the Doppler noise signal. It has no effect on the time averaged velocity but appears as an additional noise variance in the normal Reynolds stress terms:

$$\overline{V^2} = \overline{\langle V \rangle^2} + \sigma^2. \tag{14}$$

In Fig. 2, the deviation of the velocity spectra from the Kolmogorov spectrum originates from the additional contribution of the noise spectrum. Even if the number npp is increased by a factor of 4, the spectra (represented by the two crossed curves) decay slower than the expected $-5/3$ slope. Furthermore, the temporal resolution for npp = 16 is reduced to (1/11.7) s, which is rather low for an accurate TKE dissipation rate estimate of the inertial range. This undesired effect is the principal reason for the limited TKE and TKE dissipa-

tion rate measurements in field studies (Voulgaris and Trowbridge 1998; Blanckaert and Lemmin 2006; Hurther and Lemmin 2001). As will be shown below, the bifrequency method reduces this effect and at the same time maintains high temporal resolution that is necessary for reliable TKE budget estimates.

c. The bifrequency Doppler noise reduction method

The bifrequency method consists of estimating quasi-simultaneously the quasi-instantaneous velocities at two different carrier frequencies from the same sample volume:

$$V_1(t) = \langle V\rangle(t) + n_1(t),$$
$$V_2(t) = \langle V\rangle(t) + n_2(t), \tag{15}$$

where V_1 and V_2 are the instantaneous velocities measured nearly simultaneously with the carrier frequencies, $f_c = f_1$ and $f_c = f_2$, respectively. Each velocity component is composed of the sum of the same spatially averaged velocity and the respective noise contributions. The time-averaged noise contributions are negligible and therefore

$$\overline{V_1} = \overline{V_2} = \overline{\langle V\rangle}. \tag{16}$$

Assuming that the noise signals have white noise characteristics, the crossed velocity spectrum becomes

$$S_{V_1V_2} = \int_{-\infty}^{+\infty} R_{\langle V\rangle\langle V\rangle}(\tau)\exp(-i2\pi f\tau)\,d\tau + \int_{-\infty}^{+\infty} R_{n_1n_2}(\tau)\exp(-i2\pi f\tau)\,d\tau = S_{\langle V\rangle\langle V\rangle}, \tag{17}$$

with $S_{n_1n_2} = \int_{-\infty}^{+\infty} R_{n_1n_2}(\tau)\exp(-i2\pi f\tau)d\tau = 0$, because the white noise signals are random and statistically independent. The associated normal Reynolds stress term can be estimated from the covariance as

$$\overline{V_1V_2} = \int_0^{+\infty} S_{V_1V_2}\,df = \overline{V_1^2} - \sigma^2 = \overline{V_2^2} - \sigma^2 = \overline{\langle V\rangle^2}, \tag{18}$$

where the Doppler noise effect is suppressed; σ^2 is the noise variance. If the above reasoning is correct, the crossed-velocity spectrum should decay with a $-5/3$ slope over a much wider frequency band than the autovelocity spectra presented in Fig. 2. The $-5/3$ slope should be constant until it reaches a frequency limit, after which it should decay faster because of the spatial averaging effect. These aspects will be investigated in section 4c.

The bifrequency method will be compared to the method proposed by Garbini et al. (1982). In this case, the crossed spectrum is calculated from the velocity signals at two consecutive locations in the profile:

$$S_{V_1^zV_1^{z+1}} = S_{\langle V\rangle^z\langle V\rangle^{z+1}} \quad \text{with} \quad S_{n_1^zn_1^{z+1}} = 0. \tag{19}$$

$$\int_0^{+\infty} S_{V_1^zV_1^{z+1}}\,df = \overline{\langle V\rangle^z\langle V\rangle^{z+1}}. \tag{20}$$

As with the bifrequency method, the Doppler noise contribution is eliminated. However, the TKE contained in velocity components that are uncorrelated between two consecutive sample volumes are also eliminated. This is typically the case for isotropic flow structures that are smaller than the sample volume. Figure 2 shows the application of Garbini's method to the OGT experiment for the two carrier frequencies ($f_1 = 1.25$ and $f_2 = 1.67$ MHz) at high temporal resolution (npp = 4). It underestimates the turbulent energy in the higher frequency range. Furthermore, the application of this method requires a profiling ability that is not yet available with commercial bistatic ADV systems (Nortek, Sontek).

4. Results and discussion

Profiles of TKE, the TKE rate, and the corresponding spectra obtained with a standard monofrequency system will be compared to estimates using the new bifrequency method with the same hardware system. Two frequency pairs will be tested using the bifrequency method. Results obtained by the application of the method proposed by Garbini et al. (1982) are also shown. The values obtained from the application of Eqs. (1) and (2) with Eqs. (3) and (4) (Matsunaga et al. 1999) will serve as reference for the "true" TKE and TKE dissipation rate profiles. For all data presented below, the time series are averaged over 240 s with a velocity time resolution of (1/46.7) s obtained for npp = 4. This value provides sufficient resolution for the analysis of the inertial range.

a. TKE profile

The following approximation, valid for OGT, is applied:

$$k = 0.5(\overline{u^2} + \overline{v^2} + \overline{w^2}) = (3.1/2)\overline{w^2},$$
$$\text{with} \quad \overline{u^2} + \overline{v^2} = 2(1.05\overline{w^2}), \tag{21}$$

where u, v, and w are the turbulent velocity components in the horizontal (u and v) and the normal directions, respectively. An anisotropy of less than 5% between

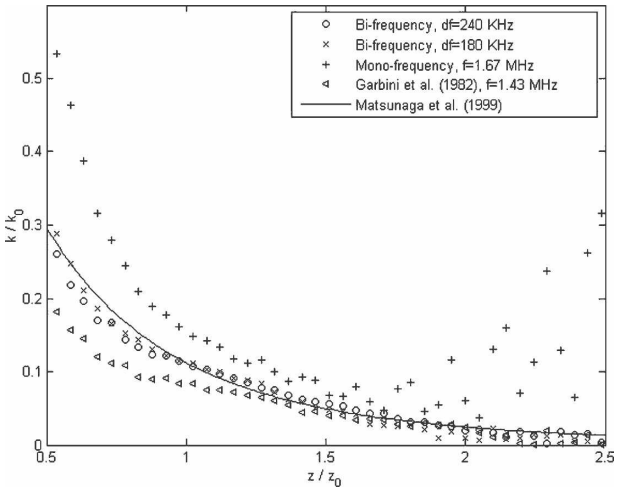

FIG. 3. Comparison of profiles of normalized TKE.

the horizontal and normal components was measured by Hopfinger and Toly (1976) in the same tank configuration. Figure 3 shows the profiles of normalized TKE with normalized distance z/z_0 from the oscillating grid. As presented in section 2a, the value of z_0 is calculated with $z_0 = k_0^{3/2}\varepsilon_0^{-1}$.

Both bifrequency results agree well with the theoretical TKE values, whereas the monofrequency method overestimates them and the Garbini method underestimates them. The differences between the bifrequency and the Garbini results decrease with increasing distance. The monofrequency results show a similar trend until $z/z_0 = 1.5$. Above this value, the deviation from the theoretical values increases. This shows the efficiency of cross-correlation techniques that are able to extract the physical velocity information even when noise dominates the raw velocity signal.

The tendency to obtain converging results with the bifrequency method and the Garbini method can be explained by the increasing turbulent scales with distance from the grid in OGT. This implies that at the location where the TKE values between the two methods coincide, small-scale turbulent eddies are larger than the size of the sample volume. In this case, the spatial covariance contains most of the physical velocity signal. In the range $z/z_0 < 1.5$, the lower TKE found in spatial covariance is due to the loss of TKE of isotropic flow structures smaller than the sample volume. This reflects the lack of spatial resolution when using a spatial decorrelation method.

b. TKE dissipation rate profiles

In this section we investigate the capacity of ABS to estimate profiles of the TKE dissipation rate in OGT. We will compare the standard method (monofrequency without noise correction), the Garbini method, and the bifrequency method for two pairs of frequencies, with the semitheoretical k–ε solution proposed by Matsunaga et al. (1999). The accurate measurement of this quantity is of great importance for most hydrodynamic field studies, since it appears as a local loss term in the energy budget. On the other hand, the TKE dissipation rate is difficult to measure accurately, because the inertial range is well established in the higher spectral range with a strong rate of decay of $-5/3$. As a result, the measuring system requires a wide spectral bandwidth unaffected by noise. To avoid an incorrect interpretation of the noise affected measurements, thorough knowledge of the underlying measurement physics is required. Here we present a simple method to reduce the noise dependence that does not require knowledge of the underlying physics and that can be implemented in all types of ADVs with minor system modification.

The most frequently used relation for the TKE dissipation rate is derived from the expression of the turbulent velocity spectrum in the inertial range (Nezu and Nakagawa 1993):

$$\varepsilon = C_1 \frac{(\overline{w^2})^{3/2}}{L_t}; \tag{22}$$

C_1 decreases with the turbulent Reynolds number Re_t, based on the integral scale and the rms velocity. It reaches a constant value that is slightly lower than unity for $\mathrm{Re}_t > 100$ (Rotta 1972; Nezu and Nakagawa 1993). Here, L_t is the integral scale determined by the integrated spatial autocorrelation function in the vertical direction for the turbulent w component. For OGT it is found to vary linearly with distance from the grid (Hopfinger and Toly 1976; Brumley and Jirka 1987; Matsunaga et al. 1999) with an empirical factor of about 0.16. At each measurement location from the grid, we determine the local value of C_1 using the calculations by Rotta (1972). The integral scale can be directly estimated because of the instantaneous profiling ability of the ADVP.

Figure 4 shows the application of Eq. (2) using ε_0 in Eqs. (3) and (4) as the normalization parameter. The curve represented by crosses corresponds to the standard method. The values are considerably higher than the model values confirming the presence of Doppler noise in the raw velocity signal. The curves for the bifrequency method are both in much better agreement with the theoretical result because of the suppression of the Doppler noise. However, it is rather striking to find higher values of TKE dissipation rates with Garbini's method, whereas the associated TKE values shown in

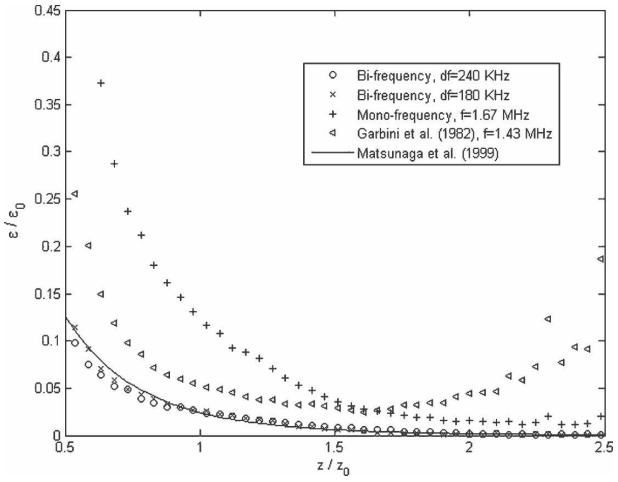

FIG. 4. Comparison of profiles of normalized TKE dissipation rate using Eq. (22).

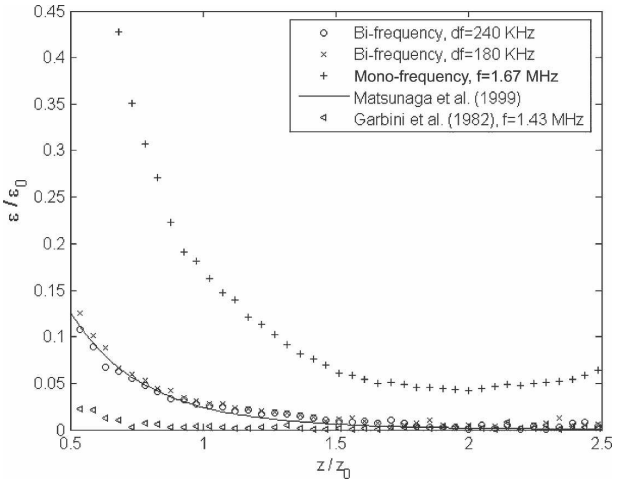

FIG. 5. Comparison of profiles of normalized TKE dissipation rate using Eq. (23).

Fig. 3 are lower than the model and the bifrequency results. This can be explained by the combined effects of the underestimated integral scale L_t and the overestimated constant C_1. Both contribute to an increase of the TKE dissipation rate in Eq. (22), which is higher than the effect of the underestimated TKE. The high C_1 with values up to 3 originates from the strong increase of C_1 with decreasing Reynolds number Re_t (Nezu and Nakagawa 1993). At a fixed distance from the grid, the Re_t obtained with the Garbini method is indeed lower than that of the other methods.

The previous discussion has shown the limits of the comparison test when using the semiempirical formula given by Eq. (22). The identification of the dominant source of error is particularly difficult, because the relation depends on three different parameters. Furthermore, the constant C_1 is determined by an empirical function of unknown accuracy. To examine more precisely the benefits of the proposed correction method, the following relation is used:

$$\varepsilon = 15\nu\overline{\left(\frac{\partial w}{\partial z}\right)^2}. \tag{23}$$

The last term on the rhs of Eq. (23) is the mean square turbulent flow divergence. This approximation is valid for isotropic turbulence found in the far field of OGT. Since no empirical constant is introduced, this is a fairly direct estimate of ε. Figure 5 shows that the standard method is strongly affected by the presence of Doppler noise. The application of the Garbini method is in better agreement with the expected loss of resolved TKE (see Fig. 3) due to the lack in spatial resolution for $z/z_0 < 1.5$. It also corresponds to the underestimated power contained in the associated spectrum shown in Fig. 2.

The two bifrequency results agree well with the model results. Furthermore, the results obtained with the two bifrequency methods are in good agreement with the two models for the TKE dissipation rate [Eqs. (22) and (23)]. The relative differences with the theoretical model results will be discussed in section 4d.

c. *Turbulent velocity spectra*

A better demonstration of the effect of the bifrequency method is given by the analysis of velocity spectra. Figure 6 shows three spectra at different distances from the grid center. For each case we compare the spectrum of the raw velocity data given by Eq. (12) to the corrected spectrum [Eq. (17)] using the bifrequency method for $df = 180$ kHz. A log–log representation is chosen to facilitate the comparison with the $-5/3$ decay slope with frequency, valid for isotropic turbulence in the inertial range. To be able to resolve an important fraction of the inertial range, the parameter npp is set to 4, which results in a Nyquist frequency of 46.9 Hz. This limit is higher than the Nyquist frequencies commonly set in ADVs (usually below a value of 32 Hz in commercial systems). Whether this high spectral resolution is physically meaningful will be addressed below.

The improvements due to the bifrequency method are obvious in Fig. 6. The uncorrected and corrected spectra are in good agreement in the lower spectral range up to 2 or 3 Hz. In this range, both spectra decay with a slope close to $-5/3$, which is due to the isotropic nature of OGT even at low frequencies. For higher frequencies, the uncorrected spectra deviate significantly from the $-5/3$ slope, whereas the slope of the corrected spectra is unchanged up to 20 Hz. Above this

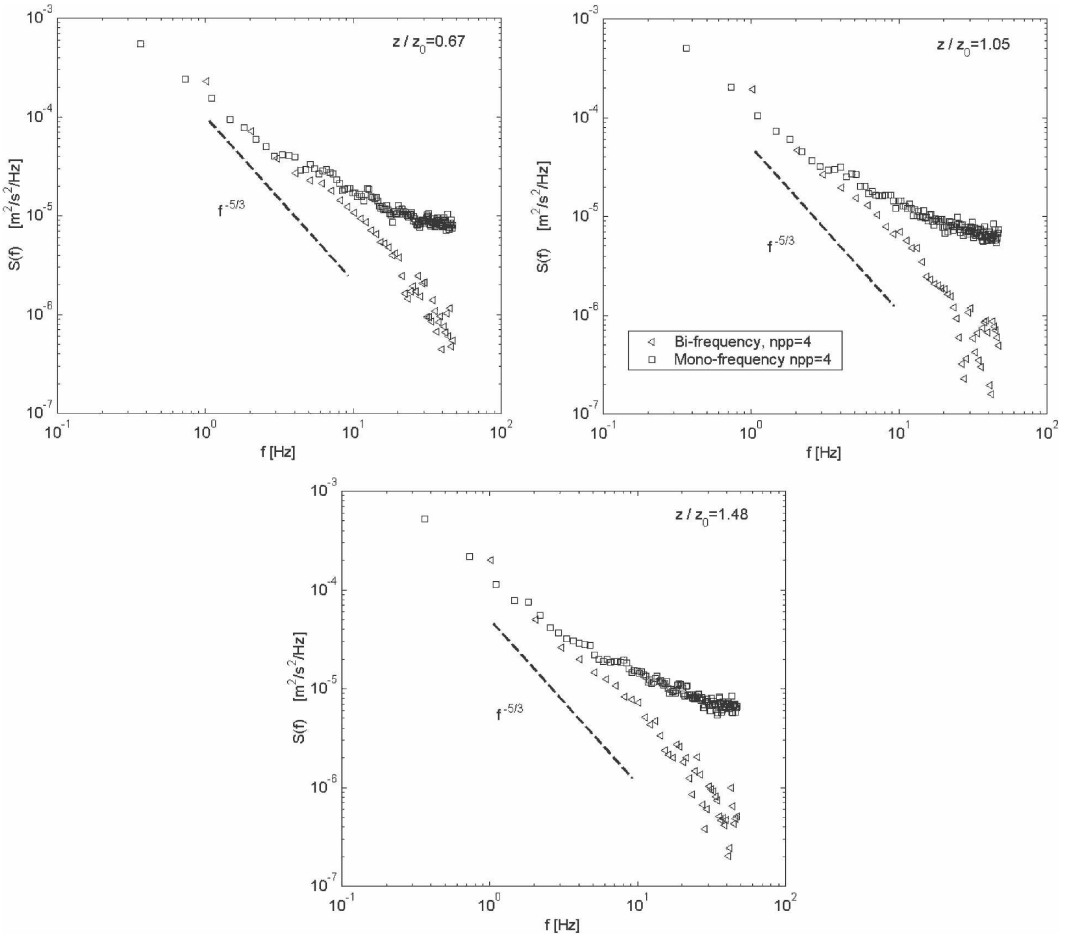

FIG. 6. Turbulent velocity spectra at three locations in the far field of the OGT. Spectra are uncorrected (monofrequency) and corrected, using the bifrequency method with df = 180 kHz.

limit, the decay slope increases abruptly until the Nyquist frequency. This change in slope results from the spatial averaging effect of the velocity over the sampling volume. This limit primarily depends on the characteristics of the transducer but can also relate to the minimal signal-to-noise ratio of the system. For the present system, the gain in frequency range is on the order of a decade.

d. Error analysis

The present error analysis is applied to the normalized TKE dissipation rate measurements using the theoretical model results by Matsunaga et al. (1999) as reference values. A best linear fit between the different experimental estimates and the reference is calculated using a least mean square (LMS) constrain. Figure 7 presents the experimental results versus the model results for the two bifrequency methods with npp = 4, the standard (monofrequency) method for f_c = 1.67 MHz with npp = 4 and npp = 32, and the Garbini method with npp = 4. The standard method with npp = 32 corresponds to a setting frequently used in commercial ADV systems. Also shown is the fitted curve with the associated LMS error. The errors for both bifrequency methods are less than 10%, even below 5% for df = 180 kHz. For npp = 4, the errors with the Garbini and standard methods are as high as 200% and 500%, respectively. However, if compared to the common ADVP setting with npp = 32 for the standard method, this error is reduced to 20%. The bifrequency Doppler noise suppression method is shown to provide accurate TKE and TKE dissipation rate estimates in the fully developed inertial range of turbulent spectra. Standard ADVs working in monofrequency mode are rather limited in this respect.

e. Turbulent microscales

The ability to resolve the turbulent microscales is indicated by the ratio between the Taylor and Kolmo-

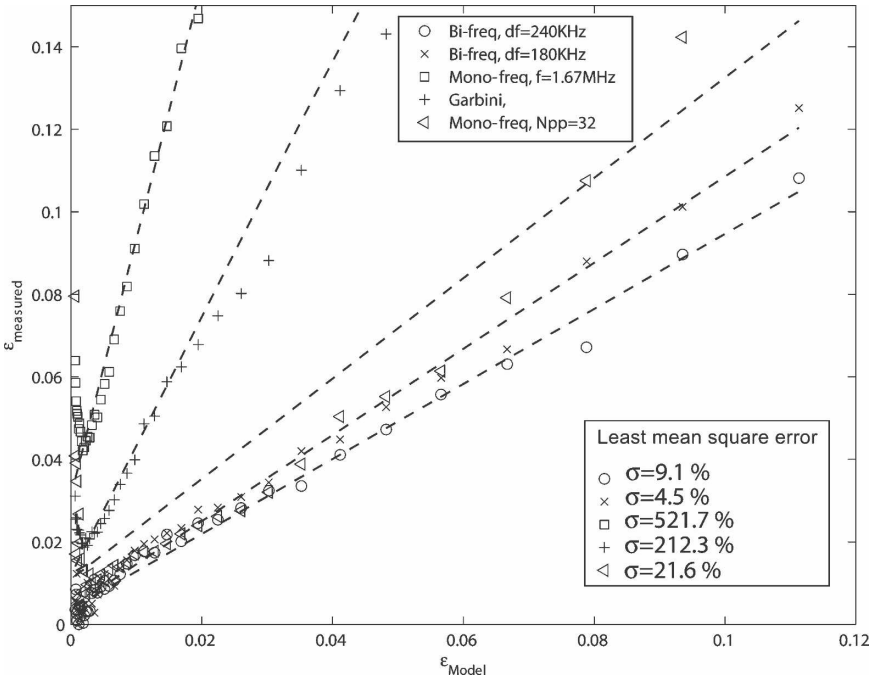

FIG. 7. Measured vs model (Matsunaga et al. 1999) predicted values of TKE dissipation rate.

gorof microscales as a function of the turbulent Reynolds number Re_t (based on the integral length scale and the rms velocity). The two bifrequency results are shown in Fig. 8. It can be seen that the ratio increases linearly in a log–log representation with a slope of roughly 1/4. An LMS fitted curve with a 1/4 slope is also presented. The mean-squared correlation coefficient of the two results is higher than 93%. This demonstrates the ability to resolve small-scale turbulent processes with field-adapted ADV systems when an adequate Doppler noise reduction method is used.

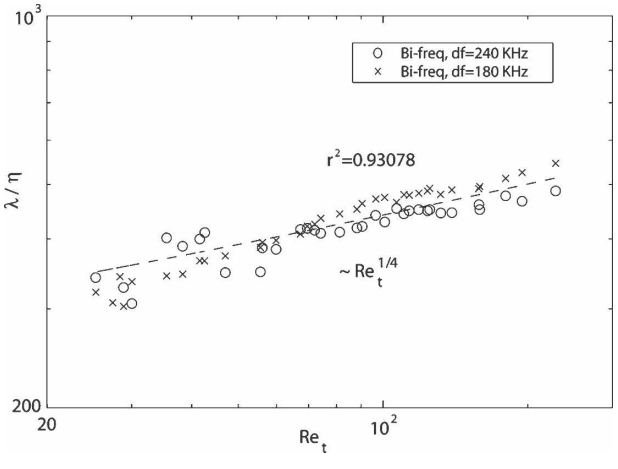

FIG. 8. Measured ratio between Taylor microscale and Kolmogorov scale vs Reynolds number Re_t; Re_t is based on the integral scale and the rms velocity. The results using the two bifrequency methods are compared with the 1/4 power law. The squared correlation coefficient is the mean of the two results.

5. Conclusions

Acoustic Doppler velocimetry is commonly used in nearshore, coastal ocean, estuary, river, and lake environments. Compared to measurements in shear-dominated currents found in estuaries or rivers, measurements in diffusive isotropic flow fields such as those generated by wave breaking in surfzones are particularly difficult with ADV systems.

The present study aims to improve these ADV turbulence measurements. A novel noise reduction method was developed using two slightly different carrier frequencies for the simultaneous and instantaneous estimates of two Doppler signals in the same sample volume. The two signals are shown to be affected by the Doppler noise inherent to the measuring principle. It is produced by the deviation of the targets' positions from their mean position in the sample volume. This results in an additional random Doppler phase and associated random velocity fluctuation known as the Doppler noise term.

It is shown that a relative shift of 10% between carrier frequencies of two Doppler signals is sufficient to

obtain random velocity noises that are statistically independent for two simultaneous estimates. The calculation of the velocity cross correlation allows suppressing the Doppler noise terms affecting the TKE, the TKE dissipation rate, and the velocity spectra.

Two different frequency shifts were tested. The experiments were conducted in an oscillating grid turbulence (OGT) tank in order to produce well-controlled isotropic turbulence at each horizontal plane in the far field above the grid. For both settings, the residual relative errors on the TKE and the TKE dissipation rate were less than 10% when the bifrequency method was used. Furthermore, this bifrequency method can suppress the Doppler noise even when the Doppler phase is averaged over only 4–8 consecutive pings. This corresponds to a gain of a factor of 4–8 in time resolution, which improves the inertial range resolution of the turbulent spectra. Thus, compared to monofrequency methods, the universal $-5/3$ decay slope in the inertial range is extended by a decade to an upper limit of about 20 Hz. Above this limit, spatial averaging effects over the sample volume result in a decay slope well below the $-5/3$ value. This limit is device-dependent and has to be determined for each ADV system. The ability to resolve the Taylor and Kolmogorov microscales with the bifrequency method is demonstrated by the good agreement of their ratio with a 1/4 power law of the Reynolds number. Therefore, the bifrequency method provides the high temporal resolution that is needed for reliable TKE budget estimates.

Since the method works with small frequency shifts relative to the central frequency of the transducer, it only requires minor software modifications for its implementation in existing ADV systems. This is a major technical advantage over previously proposed noise correction methods, which require a profiling ability (Garbini et al. 1982) or the use of additional hardware components (receiver and associated hardware; Hurther and Lemmin 2001; Blanckaert and Lemmin 2006).

Acknowledgments. We are thankful for comments of two anonymous reviewers that helped to improve the quality of the paper. This work was funded by the PNEC (Programme National de l'Environnement Côtier) and the CNRS-INSU-DT "Equipement Milourd." The authors are grateful for their support.

REFERENCES

Betteridge, K. F. E., P. S. Bell, P. D. Thorne, and J. J. Williams, 2006: Evaluation of a triple-axis coherent Doppler velocity profiler for measuring near-bed flow: A field study. *J. Atmos. Oceanic Technol.,* **23,** 90–106.

Blanckaert, K., and H. J. De Vriend, 2004: Secondary flow in sharp open-channel bends. *J. Fluid Mech.,* **498,** 353–380.

——, and U. Lemmin, 2006: Means of noise reduction in acoustic turbulence measurements. *J. Hydraul. Res.,* **44,** 1–37.

Bouvard, M., and H. Dumas, 1967: Application de la méthode de fil chaud à la mesure de la turbulence dans l'eau (in French). *La Houille Blanche,* **22,** 257–278.

Brumley, B. H., and G. H. Jirka, 1987: Near-surface turbulence in a grid-stirred tank. *J. Fluid Mech.,* **183,** 235–263.

Davies, A. G., and P. D. Thorne, 2005: Modeling and measurement of sediment transport by waves in the vortex ripple regime. *J. Geophys. Res.,* **110,** C05017, doi:10.1029/2004JC002468.

De Silva, I. P. D., and H. J. S. Fernando, 1992: Some aspects of mixing in a stratified turbulent patch. *J. Fluid Mech.,* **240,** 601–625.

Elgar, S., B. Raubenheimer, and R. T. Guza, 2005: Quality control of acoustic Doppler velocimeter data in the surfzone. *Meas. Sci. Technol.,* **16,** 1889–1893.

Garbini, J. L., F. K. Forster, and J. E. Jorgensen, 1982: Measurement of fluid turbulence based on pulsed ultrasound techniques. Part I: Analysis. *J. Fluid Mech.,* **118,** 445–470.

Gratiot, N., H. Michallet, and M. Mory, 2005: On the determination of the settling flux of cohesive sediments in a turbulent fluid. *J. Geophys. Res.,* **110,** C06004, doi:10.1029/2004JC002732.

Hay, A. E., and J. Sheng, 1992: Vertical profiles of suspended sand concentration and size from multifrequency acoustic backscatter. *J. Geophys. Res.,* **97,** 15 661–15 677.

Hoefel, F., and S. Elgar, 2003: Wave-induced sediment transport and sandbar migration. *Science,* **299,** 1885–1887.

Hopfinger, E. J., and J. A. Toly, 1976: Spatially decaying turbulence and its relation to mixing across density interfaces. *J. Fluid Mech.,* **78,** 155–175.

Hurther, D., and U. Lemmin, 1998: A constant-beam-width transducer for 3D acoustic Doppler profile measurements in open-channel flows. *Meas. Sci. Technol.,* **9,** 1706–1714.

——, and ——, 2000: Shear stress statistics and wall similarity analysis in turbulent boundary layers using a high resolution 3D ADVP. *IEEE J. Oceanic Eng.,* **25,** 446–457.

—— and ——, 2001: A correction method for mean turbulence measurements with a 3D acoustic Doppler velocity profile. *J. Atmos. Oceanic Technol.,* **18,** 446–458.

——, and ——, 2003: Turbulent particle flux and momentum flux statistics in suspension flow. *Water Resour. Res.,* **39,** 1139, doi:10.1029/2001WR001113.

——, H. Michallet, and X. Gondran, 2007: Turbulent measurements in the surf zone suspension. *J. Coastal Res.,* **SI50,** 297–301.

Kim, S.-C., C. T. Friedrichs, J. P.-Y. Maa, and L. D. Wright, 2000: Estimating bottom stress in a tidal boundary layer from acoustic Doppler velocimeter data. *J. Hydraul. Eng.,* **126,** 399–406.

Lane, S. N., and Coauthors, 1998: Three-dimensional measurement of river channel flow processes using acoustic Doppler velocimetry. *Earth Surf. Processes Landforms,* **23,** 1247–1267.

Lhermitte, R., and U. Lemmin, 1994: Open-channel flow and turbulence measurement by high-resolution Doppler sonar. *J. Atmos. Oceanic Technol.,* **11,** 1295–1308.

López, F., and M. H. Garcia, 1999: Wall similarity in turbulent open-channel flow. *J. Eng. Mech.,* **125,** 789–796.

Loupas, T., and R. W. Gill, 1994: Making full use of the information present in the backscattered RF echoes. *IEEE Trans. Ultrason. Ferroelectr. Freq. Control,* **41,** 522–531.

Matsunaga, N., Y. Sugihara, T. Komatsu, and A. Masuda, 1999:

Quantitative properties of oscillating-grid turbulence in a homogeneous fluid. *Fluid Dyn. Res.,* **25,** 147–165.

Nezu, I., and H. Nakagawa, 1993: *Turbulence in Open-Channel Flows*. A. A. Balkema, 281 pp.

Nikora, V. I., and D. G. Goring, 2000: Flow turbulence over fixed and weakly mobile gravel beds. *J. Hydraul. Eng.,* **126,** 679–690.

Rotta, J. C., 1972: *Turbulente Strömungen, eine Einführung in die Theorie und ihre Anwendungen*. B. G. Teubner, 267 pp.

Rouse, H., and J. Dodu, 1955: Diffusion turbulente à travers une discontinuité de densité. *Houille Blanche,* **10,** 522–532.

Sénéchal, N., P. Bonneton, and H. Dupuis, 2002: Field experiment on secondary wave generation on a barred beach and the consequent evolution of energy dissipation on the beach face. *Coastal Eng.,* **46,** 233–247.

Thompson, S. M., and J. Turner, 1975: Mixing across an interface due to turbulence generated by an oscillating grid. *J. Fluid Mech.,* **67,** 349–368.

Thorne, P. D., and D. M. Hanes, 2001: A review of acoustic measurement of small-scale sediment processes. *Cont. Shelf Res.,* **22,** 603–632.

Trowbridge, J., and S. Elgar, 2001: Measurements of surfzone turbulence. *J. Phys. Oceanogr.,* **31,** 2403–2417.

Turner, J., 1968: The influence of molecular diffusivity on turbulent entrainment across a density interface. *J. Fluid Mech.,* **33,** 639–656.

Ura, M., T. Komatsu, and N. Matsunaga, 1987: Entrainment due to oscillating-grid turbulence in two-layered fluid. *Turbulence Measurements and Flow Modeling,* C. J. Chen, L. D. Chen, and F. M. Holly Jr., Eds., Hemisphere Publishing, 109–118.

Voulgaris, G., and J. H. Trowbridge, 1998: Evaluation of the Acoustic Doppler Velocimeter (ADV) for turbulence measurements. *J. Atmos. Oceanic Technol.,* **15,** 272–289.

Zappa, C. J., P. A. Raymond, E. A. Terray, and W. R. McGillis, 2003: Variation in surface turbulence and the gas transfer velocity over a tidal cycle in a macro-tidal estuary. *Estuaries,* **26,** 1401–1415.

Zedel, L., A. E. Hay, R. Cabrera, and A. Lohrmann, 1996: Performance of a single-beam pulse-to-pulse coherent Doppler profiler. *IEEE J. Oceanic Eng.,* **21,** 290–297.